Cell

Inhibition of Retrograde Transport Protects Mice from Lethal Ricin Challenge

Bahne Stechmann,[1,4] Siau-Kun Bai,[1,4] Emilie Gobbo,[5] Roman Lopez,[6] Goulven Merer,[6] Suzy Pinchard,[7] Laetitia Panigai,[7] Danièle Tenza,[2,3,4] Graça Raposo,[2,3,4] Bruno Beaumelle,[8] Didier Sauvaire,[7] Daniel Gillet,[5,*] Ludger Johannes,[1,4,*] and Julien Barbier[5]

[1]Traffic, Signaling, and Delivery Laboratory
[2]Structure and Membrane Compartments Laboratory
[3]Cell and Tissue Imaging Facility (Infrastructures en Biologie Sante et Agronomie)
Centre de Recherche, Institut Curie, 26 rue d'Ulm, 75248 Paris Cedex 05, France
[4]Unité Mixte de Recherche 144, Centre National de la Recherche Scientifique, France
[5]Laboratoire de Toxinologie Moleculaire et Biotechnologies, Service d'Ingenierie Moleculaire des Proteines
[6]Laboratoire de Chimie Bioorganique, Service de Chimie Bio-organique et de Marquage
Institut de Biologie et de Technologies de Saclay, Direction des Sciences du Vivant, Commissariat a l'Energie Atomique et aux Energies Alternatives, F-91191 Gif sur Yvette, France
[7]Unite Controles de Bioactivite et Radioanalyse, French Health Products Safety Agency (Afssaps French Official Medicines Control Laboratory), Direction des Laboratoires et des Controles, 635 rue de la Garenne, 34740 Vendargues, France
[8]Centre d'etudes d'agents Pathogenes et Biotechnologies pour la Sante, Centre National de la Recherche Scientifique, Unité Mixte de Recherche 5236, Case 100, Université Montpellier 2, 34095 Montpellier, France
*Correspondence: daniel.gillet@cea.fr (D.G.), ludger.johannes@curie.fr (L.J.)
DOI 10.1016/j.cell.2010.01.043

SUMMARY

Bacterial Shiga-like toxins are virulence factors that constitute a significant public health threat worldwide, and the plant toxin ricin is a potential bioterror weapon. To gain access to their cytosolic target, ribosomal RNA, these toxins follow the retrograde transport route from the plasma membrane to the endoplasmic reticulum, via endosomes and the Golgi apparatus. Here, we used high-throughput screening to identify small molecule inhibitors that protect cells from ricin and Shiga-like toxins. We identified two compounds that selectively block retrograde toxin trafficking at the early endosome-TGN interface, without affecting compartment morphology, endogenous retrograde cargos, or other trafficking steps, demonstrating an unexpected degree of selectivity and lack of toxicity. In mice, one compound clearly protects from lethal nasal exposure to ricin. Our work discovers the first small molecule that shows efficacy against ricin in animal experiments and identifies the retrograde route as a potential therapeutic target.

INTRODUCTION

The plant toxin ricin and the bacterial Shiga toxins are members of a family of protein toxins that transit along the retrograde pathway to exert their deleterious effects on eukaryotic cells (Johannes and Popoff, 2008; Lord et al., 2003; Sandvig and van Deurs, 2005). Ricin from the seeds of the castor oil plant *Ricinus communis* is classified as a potential bioterror agent for which no treatment is available, and, as such, constitutes a concern for health authorities (Audi et al., 2005). The family of Shiga toxins includes Shiga toxin produced by *Shigella dysenteriae*, and Shiga-like toxins 1 (Stx1) and 2 (Stx2) from enterohemorrhagic *Escherichia coli* strains (for a review, see Johannes and Römer, 2010). While Shiga toxin and Stx1 are 99% identical, Stx1 and Stx2 share only 56% amino acid sequence identity. Infections with Shiga-like toxin (SLT) producing bacteria can cause hemorrhagic colitis, hemolytic-uremic syndrome (HUS), and death (Tarr et al., 2005).

SLTs and ricin are composed of two subunits (Johannes and Römer, 2010; Lord et al., 2003). Their A subunits have ribosomal RNA (rRNA) N-glycosidase activity and catalyze the removal of the same adenine at position 4324 of 28S rRNA, thereby inhibiting protein biosynthesis. By virtue of their B subunits, these toxins bind to their cell surface receptors: galactose and N-acetylgalactosamine moieties of glycoproteins and glycolipids for ricin, and the glycosphingolipid globotriaosyl ceramide (Gb3 or CD77) in the case of Stx1 and Stx2. After internalization by clathrin-dependent and independent mechanisms, these toxins are transported from early endosomes to the endoplasmic reticulum (ER), via the Golgi apparatus (Johannes and Römer, 2010; Sandvig and van Deurs, 2005). This still poorly explored transport pathway was termed the retrograde route. It is involved in a number of physiological and pathological situations ranging from morphogen gradient formations and growth factor trafficking to toxin entry and Alzheimer's disease (reviewed in Johannes and Popoff, 2008).

A critical step in the retrograde route is the escape from the endocytic pathway at the level of early endosomes (Mallard et al., 1998). This retrograde sorting process is highly selective in that only small quantities of bulk membrane and fluid phase are targeted nonspecifically from endosomes to the *trans*-Golgi network (TGN) (Snider and Rogers, 1985). A large number of proteins have been shown to be critical (reviewed in Bonifacino and Rojas, 2006; Johannes and Popoff, 2008). The current model suggests that clathrin and clathrin-binding proteins such as epsinR, AP-1, OCRL, and RME-8 are required for the formation of retrograde tubules on early endosomes. These retrograde tubules are then processed, involving the retromer complex (Bonifacino and Hurley, 2008). The fusion of retrograde transport intermediates with the TGN requires tethering factors such as golgin-97, GCC88, GCC185, and GARP, SNARE complexes involving syntaxin 16 and syntaxin 5, and the GTPase Rab6a′.

To date, there is no proven, safe treatment for ricin intoxication or complicated infections by SLT-producing *Escherichia coli* strains other than supportive care (http://emergency.cdc.gov/agent/ricin/clinicians/treatment.asp; http://www.cdc.gov/nczved/dfbmd/disease_listing/stec_gi.html). For this, the identification of compounds that inhibit endocytic toxin trafficking without exhibiting detrimental effects on cell viability and organelle integrity would be of interest. In this study, we used cell-based high-throughput screening (HTS) to identify pharmacologically active compounds able to protect cells from intoxication by ricin and Stx1 and 2. We identified two compounds capable of blocking specifically the early endosome-to-TGN toxin transport step without affecting endogenous retrograde cargo proteins, other intracellular trafficking pathways, or, more generally, organelle integrity. One compound, termed Retro-2, clearly protects mice from intranasal LD_{90} challenge by ricin and is particularly active to provide total protection at high doses.

RESULTS

Identification of Ricin Inhibitors by HTS

On the basis of a previously described method (Liger et al., 1997), a cell-based assay was derived for HTS of ricin inhibitors. In this assay, the inhibitory effect of ricin on protein biosynthesis of intact cells is measured through the incorporation of radioactive leucine into neosynthesized polypeptides. We screened for small molecules that restored normal levels of protein biosynthesis in the presence of ricin, i.e., that inhibited the intoxication of cells by ricin. HTS was performed on a library of 16,480 drug-like compounds at a final concentration of 25 μM (Figure 1A). Twelve compounds provided at least 10% inhibition against ricin cytotoxicity. By examining the effect of increasing ricin concentrations on protein biosynthesis in the presence of these compounds, we confirmed four hits (hit rate of 0.024%) as robust ricin inhibitors.

For reasons that will be apparent later, two lead compounds were named Retro-1 and Retro-2 and chosen for further analysis. They combined minimal apparent cellular toxicity with robust activity against ricin and SLTs (see below). Their heterocyclic structures with central imine or benzodiazepine moieties are shown in Figure 1B. Given that inhalation is believed to be the most efficient exposure route to ricin (Audi et al., 2005), their protective activity was tested by challenging human pulmonary carcinoma alveolar basal epithelial A549 cells with increasing concentrations of ricin under conditions of the HTS assay (Figure 1C). Both compounds showed significant increases in EC_{50} values, corresponding to protection factors of 4.6 ± 1.2 standard deviation (SD; n = 11) for Retro-1 and 3.6 ± 1.1 SD (n = 8) for

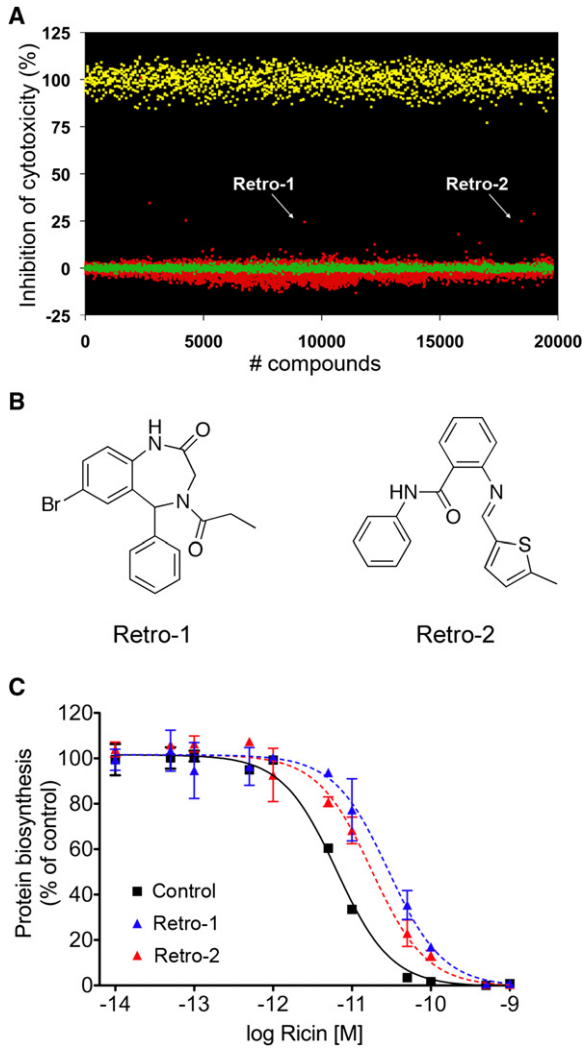

Figure 1. High-Throughput Screening for Inhibitors of Ricin Cytotoxicity

(A) Primary screen of Chembridge library. Library compounds were screened on A549 human lung carcinoma cells. Yellow dots represent positive controls (A549 cells treated with ricin in presence of 20 mM lactose, a competitive inhibitor of ricin binding). Green dots are negative controls (A549 cells treated with ricin only). Red dots correspond to A549 cells incubated with library compounds in presence of ricin. Retro-1 and Retro-2 are indicated.

(B) Chemical structures of Retro-1 and Retro-2.

(C) Intoxication of A549 cells by ricin in presence of inhibitors. Experimental conditions are the same as those described for HTS. Cells were incubated 30 min with Retro-1 and Retro-2 before addition of ricin at the indicated concentrations for 20 hr. Media was removed and replaced with DMEM containing ^{14}C-leucine at 0.5 μCi/ml for 7 hr before counting. Each data point represents the mean of duplicate ± SD of a representative experiment.

See also Figure S1 and Table S3.

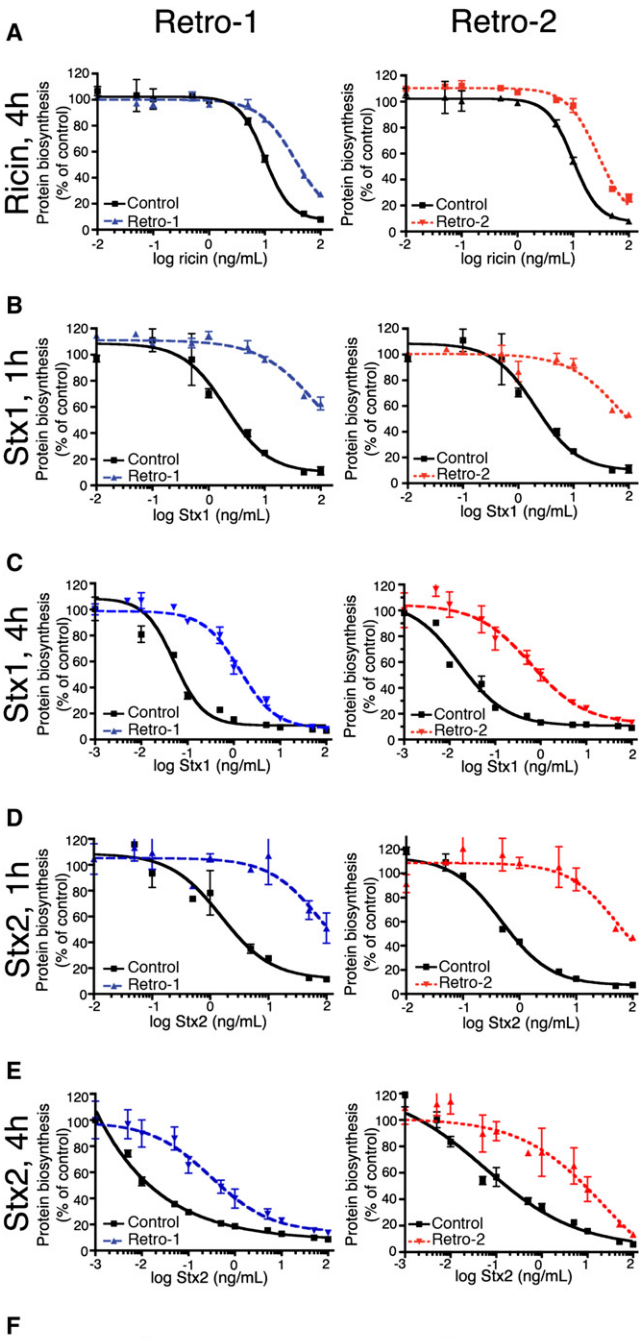

F

	Protection Factor		Protection Factor
Ricin, 4h	3.6 ± 0.1 (n=2)	Ricin, 4h	2.7 ± 0.1 (n=2)
Stx1, 1h	37 ± 10 (n=6)	Stx1, 1h	42 ± 9 (n=4)
Stx1, 4h	24 ± 2 (n=2)	Stx1, 4h	22 ± 12 (n=3)
Stx2, 1h	75 ± 25 (n=2)	Stx2, 1h	>100 (n=2)
Stx2, 4h	>100 (n=2)	Stx2, 4h	65 ± 35 (n=2)

Figure 2. Retro-1 and Retro-2 Protect HeLa Cells against Ricin, Stx1, and Stx2

(A–E) Cells were preincubated for 30 min at 37°C with DMSO (0.04%; black data points in all parts of the figure), Retro-1 (20 μM; blue, left column), or Retro-2 (20 μM; red, right column) before addition of toxin. Intoxication of HeLa cells by ricin (4 hr) (A), Stx1 (1 hr) (B), Stx1 (4 hr) (C), Stx2 (1 hr) (D), and Stx2 (4 hr) (E) are shown. Each point corresponds to the mean ± SEM of a representative experiment out of two to six determinations.

(F) Protection factors calculated over the indicated number of experiments. Means ± SEM are shown.

Retro-2. These experiments show that both compounds partially protect A549 cells against ricin exposure. A similar protective effect was observed on HeLa cells (Figure 2A, see below), demonstrating that compound activity was not restricted to a specific cell type. No additive or synergistic effects were found when A549 or HeLa cells were treated simultaneously with both compounds (Figures S1A and S1B available online). Incubation of A549 or HeLa cells with 25 μM Retro-1 or Retro-2 for as long as 4 days did not affect protein biosynthesis (Figures S1C and S1D), indicating that the compounds were not toxic at the concentrations used in this study.

No alteration of ricin activity on a 14-mer RNA template mimicking the toxin's natural ribosomal RNA substrate was detected in the presence of Retro-1 and Retro-2 (F. Becher, E. Duriez and E. Ezan, personal communication). Moreover, preincubation of ricin (or SLTs, see below) with Retro-1 or Retro-2 did not improve the compounds' protective effect, while it was found to be necessary to preincubate cells for 30 min with the compounds to obtain optimal protection (data not shown). These different sets of data therefore demonstrated that Retro-1 and Retro-2 do not inhibit the toxins directly. Rather, they appear to interfere with early stages of toxin entry into cells.

Retro-1 and Retro-2 Strongly Protect HeLa Cells against SLTs

As ricin shares with SLTs the trafficking via the retrograde route, we analyzed whether Retro-1 and Retro-2 also protected cells against these toxins. Protection experiments were performed on HeLa cells, because A549 cells do not express the Gb3 glycolipid and are thus resistant to SLTs. After pretreatment for 30 min with vehicle alone (0.04% dimethyl sulfoxide [DMSO]), or with 20 μM Retro-1 or Retro-2, cells were incubated with increasing concentrations of ricin, Stx1, or Stx2, and protein biosynthesis was then measured with radiolabeled methionine. Retro-1 and Retro-2 protected HeLa cells from a 4 hr ricin challenge (Figure 2A). Ricin toxicity on HeLa cells was reduced 3.6-fold ± 0.1-fold or 2.7-fold ± 0.1-fold (mean ± standard error of the mean [SEM]) for Retro-1 or Retro-2, respectively (Figure 2F). These values are similar to those obtained on A549 cells (Figure 1C).

For SLTs, robust inhibition of protein biosynthesis was observed on HeLa cells as early as 1 hr after toxin exposure. At this time (Figures 2B and 2D), or after 4 hr of toxin incubation (Figures 2C and 2E), Retro-1 (left column) and Retro-2 (right column) strongly protect cells against Stx1 (Figures 2B and 2C) and Stx2 (Figures 2D and 2E). Protective indexes between 22 and >100 were measured (Figure 2F). Very clearly, Retro-1 and Retro-2 inhibit HeLa cell intoxication by ricin, Stx1, and Stx2.

Retro-1 and Retro-2 Specifically Inhibit Retrograde Transport to the TGN

To analyze whether Retro-1 and Retro-2 affect intracellular toxin trafficking, we used the B subunit of Stx1, termed STxB, which

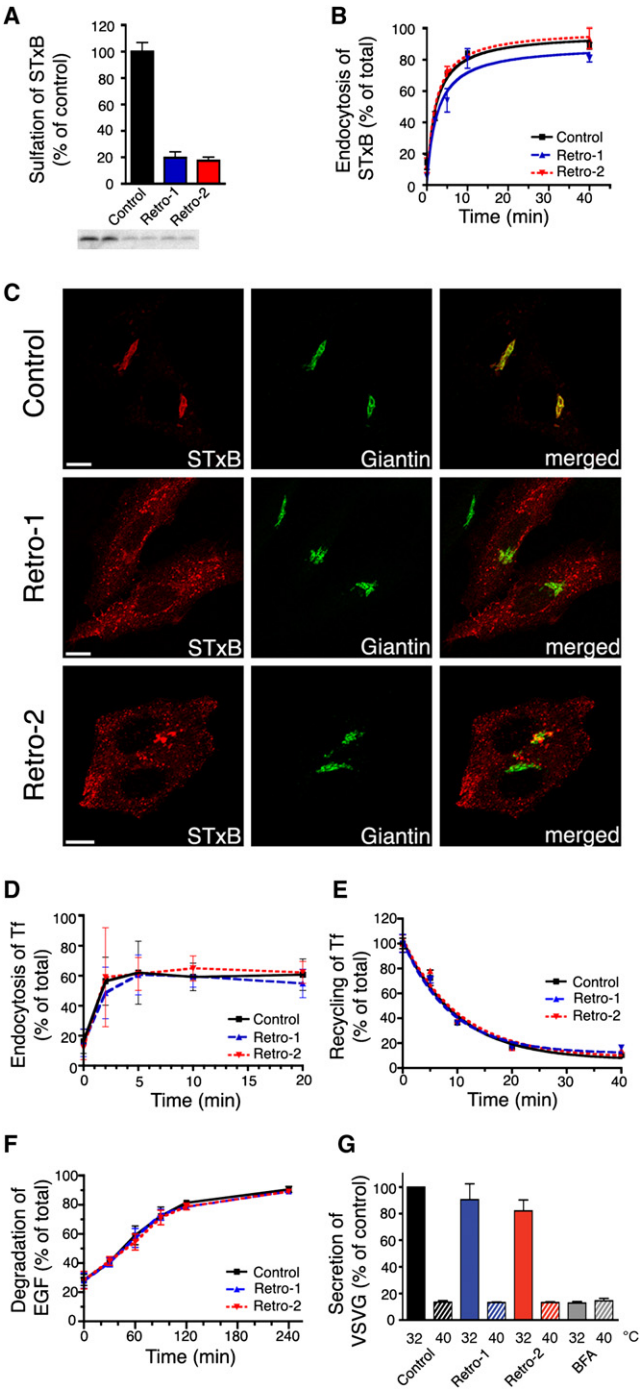

Figure 3. Retro-1 and Retro-2 Inhibit the Retrograde Transport of STxB

HeLa cells were pre-incubated with DMSO (0.04%), Retro-1 (20 μM), or Retro-2 (20 μM) for 30 min at 37°C. All subsequent incubations were carried out in the continued presence of the compounds.

(A) Sulfation assay. After binding, STxB-Sulf$_2$ (1 μM) was incubated with HeLa cells for 20 min at 37°C in the presence of radioactive sulfate. Results represent means ± SEM of three independent experiments in duplicate. The autoradiogram is from a representative experiment.

(B) Endocytosis of STxB-SS-biotin on HeLa cells. Data represent the means ± SEM (n = 3–4).

(C) Incubation of Cy3-STxB (0.5 μg/ml, red) with cells for 45 min at 37°C. The cells were then fixed and labeled for giantin (green). Scale bars represent 10 μm.

(D) Endocytosis of Tf (n = 4).

(E) Recycling of Tf (n = 2).

(F) ^{125}I-EGF-degradation in HeLa cells (n = 4).

(G) Anterograde GFP-VSVG^{ts045} transport at the indicated incubation temperatures (n = 3).

In (D–G), means ± SEM are shown. See also Figures S2 and S3.

has been developed as a morphological and quantitative biochemical tool to study various steps of toxin endocytosis and retrograde transport (Amessou et al., 2006).

In a first approach, we measured the retrograde transport of STxB to the TGN using a quantitative biochemical assay. This assay is based on the use of an STxB variant, STxB-Sulf$_2$, to which a tandem of protein sulfation sites was added by genetic fusion. Upon retrograde transport to the TGN, STxB-Sulf$_2$ becomes the substrate of TGN-localized sulfotransferase that catalyzes the posttranslational transfer of radioactive sulfate from the medium onto a tyrosyl residue of the recognition sequence. Detection of sulfated STxB-Sulf$_2$ by autoradiography thereby allows for the quantification of its retrograde arrival at the TGN. In cells pretreated for 30 min with 20 μM of Retro-1 or Retro-2, we observed a 80% ± 4% or 82% ± 3% (mean ± SEM) loss of the sulfation signal compared to vehicle-treated control cells (Figure 3A). This inhibitory effect persisted for at least 4 hr (Figure S2A). Importantly, total cellular sulfation levels (Figure S2B) and STxB binding (Figure S2C) were not affected on inhibitor-treated cells, demonstrating that sulfotransferase activity was not perturbed, that cells were in a healthy state under all conditions, and that the reduced sulfation signal was not due to reduced amounts of cell-associated STxB.

The inhibition of retrograde transport to the TGN could occur at the plasma membrane or on endosomes. To address the first possibility, we quantified the endocytic uptake of STxB in the presence of Retro-1 or Retro-2 (Figure 3B), by using a conjugate of STxB to which a biotin was linked via a thiol cleavable disulphide bond. The use of a membrane impermeable reducing agent allowed us to determine the percentage of cell surface inaccessible (internalized) STxB after various times of incubation. While preincubation for 30 min with 20 μM Retro-1 or Retro-2 clearly reduced subsequent transport of STxB to the TGN (see above), no effect on the internalization of STxB was detected under these conditions (Figure 3B), suggesting that both compounds do not exert their inhibitory effect by interfering with the cellular uptake of STxB.

The biochemical data on the inhibition of STxB transport to the TGN by Retro-1 and Retro-2 was confirmed in immunofluorescence experiments (Figure 3C). Fluorophore-tagged STxB (red) was bound on ice to vehicle-treated control or compound-treated cells (conditions as above). After washing, cells were incubated for 45 min at 37°C. In control cells, STxB (red) accumulated in perinuclear membranes that were labeled by the Golgi marker giantin (green; Figure 3C, upper panel). In cells treated either with Retro-1 (Figure 3C, middle panel) or Retro-2 (Figure 3C, lower panel), STxB no longer colocalized with giantin but appeared in peripheral structures that were evenly distributed

throughout the cytoplasm. These results confirmed that Retro-1 and Retro-2 block retrograde STxB transport to the TGN/Golgi.

Figure 3C and Figure S3 document that Golgi morphology was not visibly affected by incubation of cells with Retro-1 or Retro-2, as judged by giantin labeling. The localization of the Golgi markers CTR433 and GM130 was also unchanged (Figure S3). Furthermore, we found that the morphologies of the ER, of early (EEA1) and recycling endosomes (transferrin receptor [TfR] and Rab11), and of late endosomes/lysosomes (Lamp1) were unaffected by the compounds.

The specificity of Retro-1 and Retro-2 was further analyzed by measuring transport via a number of other routes that intersect with the early endosome-TGN interface: the biosynthetic/secretory, endocytic, and recycling pathways. These were analyzed in the presence of 20 μM of Retro-1 or Retro-2 (30 min pretreatment), conditions for which it was validated in parallel that STxB trafficking was strongly inhibited.

As we have seen above, STxB endocytosis was not affected by Retro-1 or Retro-2 (Figure 3B). On the same cells, the endocytosis of biotinylated transferrin (Tf) was analyzed, with a similar approach to the one described for STxB. Neither Retro-1 nor Retro-2 affected the clathrin-dependent endocytic uptake of Tf (Figure 3D), indicating that this major cellular internalization route was still operating in the presence of the compounds.

Tf was also used to measure recycling from early and recycling endosomes to the plasma membrane. After an uptake pulse, the quantity of remaining cell-associated Tf was determined in function of chase time at 37°C (Figure 3E). Again, neither Retro-1 nor Retro-2 had any effect.

Targeting to the late endocytic pathway was analyzed with radiolabeled epidermal growth factor (EGF). In interaction with its receptor, EGF is targeted to late endosomes/lysosomes, where the protein is degraded. This trafficking from the plasma membrane into the degrading environment of the late endocytic pathway was not affected by Retro-1 or Retro-2 (Figure 3F).

Finally, a thermosensitive vesicular stomatitis virus glycoprotein mutant fused to green fluorescent protein (GFP-VSVG^{ts045}) was used to assess the effect of Retro-1 and Retro-2 on anterograde transport along the biosynthetic/secretory pathway from the ER to the plasma membrane, via the Golgi apparatus and the TGN (Figure 3G). In these experiments, GFP-VSVG^{ts045} protein accumulated in the ER at restrictive temperature (40°C) and was then chased at permissive temperature (32°C) for 2 hr. The level of GFP-VSVG^{ts045} protein that reached the plasma membrane in vehicle-treated control cells was set to 100%. In the presence of brefeldin A, anterograde trafficking was totally inhibited, and the VSVG trafficking signal was at background levels, similar to cells that were kept at restricted temperature. Upon incubation with Retro-1 or Retro-2, GFP-VSVG^{ts045} trafficking was not significantly affected (Figure 3G).

Taken together, these results show that Retro-1 and Retro-2 have no effect on endocytosis, recycling, degradation, and secretion.

Retro-1 and Retro-2 Treatment Blocks STxB in Early Endosomes and Relocalizes Syntaxin 5

The peripheral compartments in which STxB accumulated in Retro-1 and Retro-2-treated cells were further characterized (30 min pretreatment with compounds at 20 μM). A major overlap could be found between STxB (red) and TfR (green; Figures 4A and 4C), a marker of early and recycling endosomes, and EEA1 (green; Figures 4B and 4D), a marker of early endosomes. In all these cases, 90% or 85% of TfR or EEA1-positive compartments were also labeled by STxB, respectively. In Retro-1- (Figure 4E) and Retro-2- (Figure 4F) treated cells, immunogold labeling on cryosections revealed the presence of STxB (15 nm gold particles) in tubular and vesicular structures that were also strongly labeled for TfR (10 nm gold particles), while in control (Ctr) cells, STxB efficiently accumulated in the Golgi cisternae (Figure S4A).

The retromer protein Vps26 (green) is also associated with early endosomes (Arighi et al., 2004), and we found a strong overlap (75%) with STxB (red) in Retro-1- or Retro-2-treated cells (Figures S4B and S4E). The overlap between the recycling endosomal marker Rab11 (green) and STxB (red) was less important (50% overlap; Figures S4C and S4F), but still higher than that observed for the late endosomal marker Lamp1 (green) and STxB (red; 10% overlap; Figures S4D and S4G), suggesting that when its retrograde transport to the TGN was inhibited at the level of early endosomes, STxB in part shifted to recycling endosomes but failed to reach the late endocytic pathway.

A large number of trafficking factors have been shown to regulate retrograde transport at the early endosome-TGN interface (for a review, see Johannes and Popoff, 2008). Their localization was analyzed by immunofluorescence microscopy in vehicle-treated cells and cells that were incubated for 4 hr with 20 μM of Retro-1 or Retro-2. Strikingly, the SNARE protein syntaxin 5 (green) was strongly relocalized in all compound-treated cells, while the subcellular distribution of the tethering factor golgin-97 (red) was not affected (Figure 5A). This robust relocalization could be detected as early as 30 min after the beginning of cell exposure to the compounds (Figure 5B). Retro-1 and Retro-2 did not deplete syntaxin 5 from cells, as determined by western blotting (data not shown). Syntaxin 5 regulates retrograde transport in a complex with Ykt6, GS28, and GS15 (Amessou et al., 2007; Tai et al., 2004). We found that the cellular distribution of these proteins was not affected by Retro-1 and Retro-2 (Figure 5C), suggesting that their Golgi localization is not solely dependent on syntaxin 5. Furthermore, syntaxin 5 is found in two SNARE complexes that are implicated in ER-Golgi and intra-Golgi transport: Syntaxin5/GS27/Bet1/Sec22b and Syntaxin5/GS28/Bet1/Ykt6 (Hay et al., 1998; Zhang and Hong, 2001). In cells treated with Retro-1 or Retro-2, GS27 localization was not altered (Figure 5D), again suggesting that interactions with other Golgi proteins dictate localization to Golgi membranes.

Syntaxin 6 was also displaced by Retro-1 and Retro-2 treatment of cells (Figure 5E), even if at 4 hr of compound treatment the effect appeared somewhat smaller than for syntaxin 5. At 30 min of treatment, only very few cells displayed a partially redistributed syntaxin 6 labeling pattern (Figure 5F). Since under the same conditions syntaxin 5 was already strongly affected (see above, Figure 5B), it is possible that the effect on syntaxin 6 is secondary to that on syntaxin 5. For the syntaxin 6 SNARE interacting partner syntaxin 16, a weak relocalization phenotype was observed at 4 hr of compound treatment, while the other

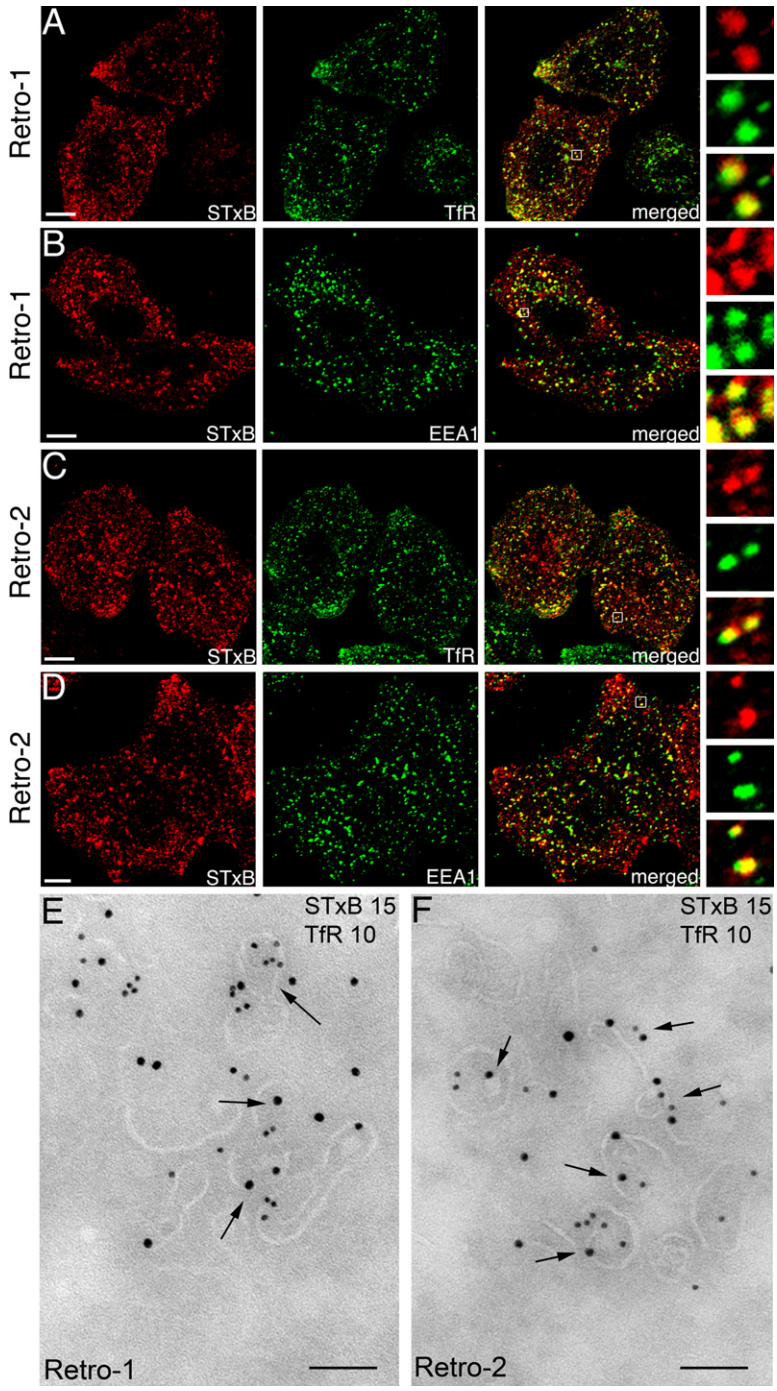

Figure 4. STxB Accumulates in Early Endosomes on Retro-1- or Retro-2-Treated Cells

(A–F) In all conditions, HeLa cells were preincubated for 30 min at 37°C with 20 μM of Retro-1 (A, B, and E) or Retro-2 (C, D, and F). All subsequent incubations were carried out in the continued presence of the compounds.

(A–D) After binding of Cy3-STxB (0.5 μg/ml, red) to cells on ice and washing, the cells were incubated for 45 min at 37°C, fixed, and labeled for the indicated proteins (green). Magnification views of boxed areas are shown on the right. Scale bars represent 10 μm.

(E and F) After binding of STxB (0.5 μM) to cells on ice and washing, the cells were incubated for 45 min at 37°C, fixed, and submitted to ultrathin cryosectioning. Sections were labeled with anti-STxB (15 nm gold particles) and anti-TfR (10 nm gold particles) antibodies and protein A gold conjugates. Scale bars represent 200 nm.

See also Figure S4.

partners of this SNARE complex that regulates retrograde transport at the early endosome-TGN interface, VAMP4 and Vti1a (Mallard et al., 2002), were not affected (Figure 5G).

The effect of Retro-1 and Retro-2 on syntaxin 5 was very specific. Indeed, the localization of none of the following retrograde trafficking factors was affected (Figure S5): clathrin light chain and clathrin heavy chain isoform CHC22; clathrin adaptors AP-1, AP-3, and epsinR; PACS-1 and PACS-2; retromer proteins Vps26, SNX1, and SNX2; GTPases Rab6 and Rab9; tethering factors golgin-97, p230, GCC185, and GCC88; and SNARE protein syntaxin 10. Furthermore, two tests revealed that phosphatidylinositol 3-phosphate (PI3P) metabolism was not affected by the compounds. First, we expressed the GFP-tagged FYVE domain of EEA1 that specifically recognizes PI3P (Hunyady et al., 2002). Retro-1 and Retro-2 did not affect the early endosomal localization of the probe, while the phosphatidylinositol 3-kinase (PI-3K) inhibitor wortmannin led to a strong relocalization (Figure S6A). Second, a Jurkat cell line with permanently activated PI-3K was transfected with a GFP-tagged PH domain construct of Akt kinase that recognizes elevated PI(3,4,5)P3 levels at the plasma membrane (Astoul et al., 2001). Again, Retro-1 and Retro-2 had no effect on PH domain localization to the plasma membrane, while the PI-3K inhibitor LY294002 as a positive control induced a strong redistribution to the cytosol (Figure S6B).

Retro-1 and Retro-2 Have No Effect on Endogenous Retrograde Cargo Proteins

Several exogenous and endogenous cargo proteins share with STxB elements of retrograde transport machinery for their efficient trafficking between early endosomes and the TGN (summarized in Johannes and Popoff, 2008). Thus, we examined whether Retro-1 and Retro-2 affected the retrograde transport of these cargoes.

Like Shiga toxin, cholera toxin is composed of a catalytic A subunit and a homopentameric B subunit (CTxB), which binds to a glycosphingolipid, and is internalized to the ER and the cytosol via the retrograde route (Sandvig et al., 2004). CTxB (green; Figure 6A, top panel) was fluorophore labeled and accumulated in perinuclear Golgi membranes (giantin, blue) after 45 min incubation with HeLa cells. Similar to STxB, the

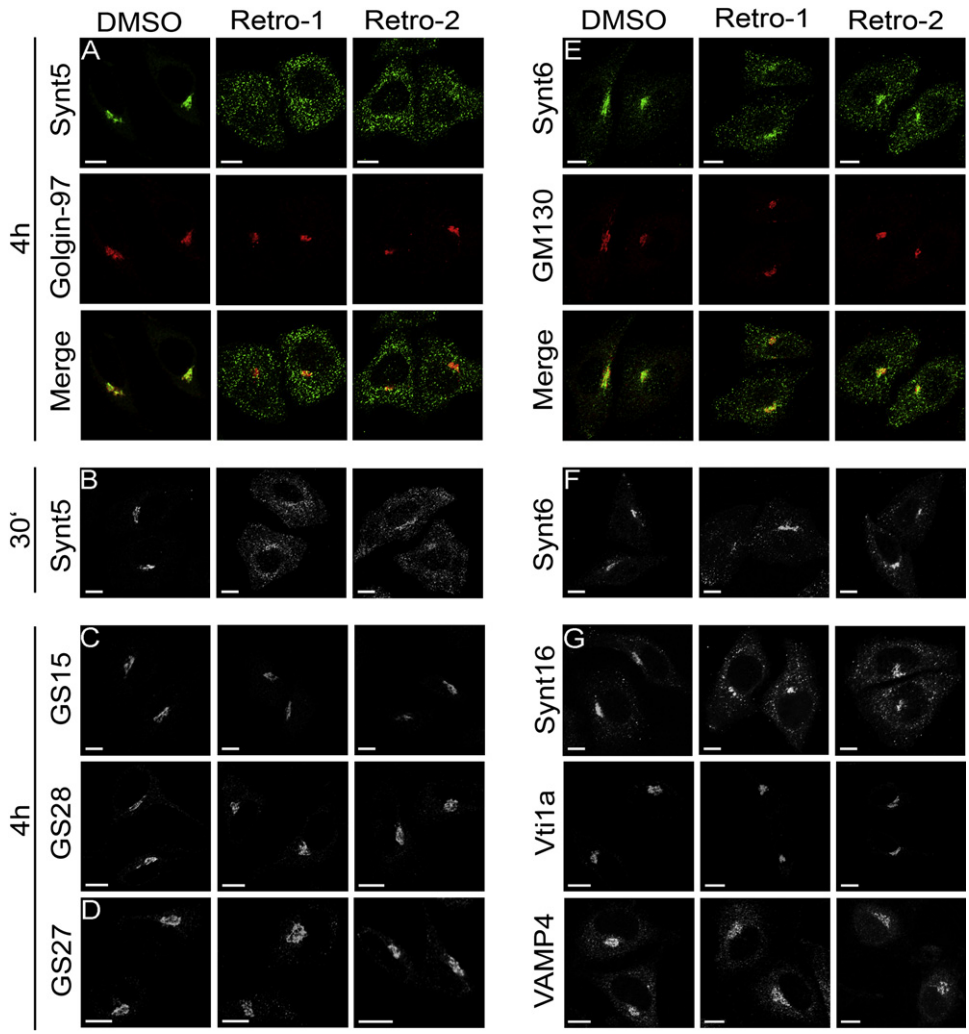

Figure 5. Retro-1 and Retro-2 Relocalize Syntaxin 5

Cells were treated for 4 hr (A, C, D, E, and G) or 30 min (B and F) with carrier (0.04% DMSO), Retro-1 or Retro-2 (20 μM), fixed, and labeled for the indicated proteins. Note the strong relocalization of syntaxin 5 that can clearly be seen after only 30 min of compound treatment. For syntaxin 6, the relocalization phenotype appears weaker and is observed systematically only at the 4 hr time point. Scale bars represent 10 μm. See also Figures S5 and S6.

accumulation of CTxB in perinuclear Golgi membranes was strongly reduced in cells that were pretreated for 30 min with 20 μM Retro-1 (Figure 6A, middle panel) or Retro-2 (lower panel), demonstrating that the cellular entry of this toxin subunit was also blocked.

The cation-independent mannose 6-phosphate receptor (CI-MPR) shuttles newly synthesized mannose 6-phosphate-tagged lysosomal enzymes from the TGN to the endosomal pathway and then returns to the TGN to retrieve additional cargo (Ghosh et al., 2003). Convergent evidence has been presented on a role in retrograde CI-MPR transport for the trafficking machinery involved in STxB uptake, even if additional complexity exists (summarized in Johannes and Popoff, 2008). In a first approach to assess the effect of Retro-1 and Retro-2 on CI-MPR trafficking, we used a cell line that expresses a GFP-tagged CI-MPR transgene (Waguri et al., 2003). Retrograde CI-MPR transport from the plasma membrane to the TGN can be followed in these cells with an antibody uptake assay that consists of adding an anti-GFP antibody into the culture medium. The antibody binds to GFP-CI-MPR at the cell surface and is then retrieved to the TGN with its antigen (Amessou et al., 2006). In the vehicle-treated control cells (Figure 6B, upper panel), the antibody (αGFP, blue) accumulated within 40 min in the perinuclear Golgi region, where it colocalized with STxB (red) and the bulk GFP fluorescence (green). Importantly, in cells that were pretreated for 60 min with 20 μM Retro-1 (middle panel) or Retro-2 (lower panel), STxB transport was strongly impaired, as described above, but the anti-MPR antibody still reached the perinuclear Golgi membranes as efficiently as in control cells, suggesting that both compounds selectively affected retrograde toxin trafficking only. In additional experiments (Figure 6C), we found that even after incubations for as long as 6 hr, 20 μM

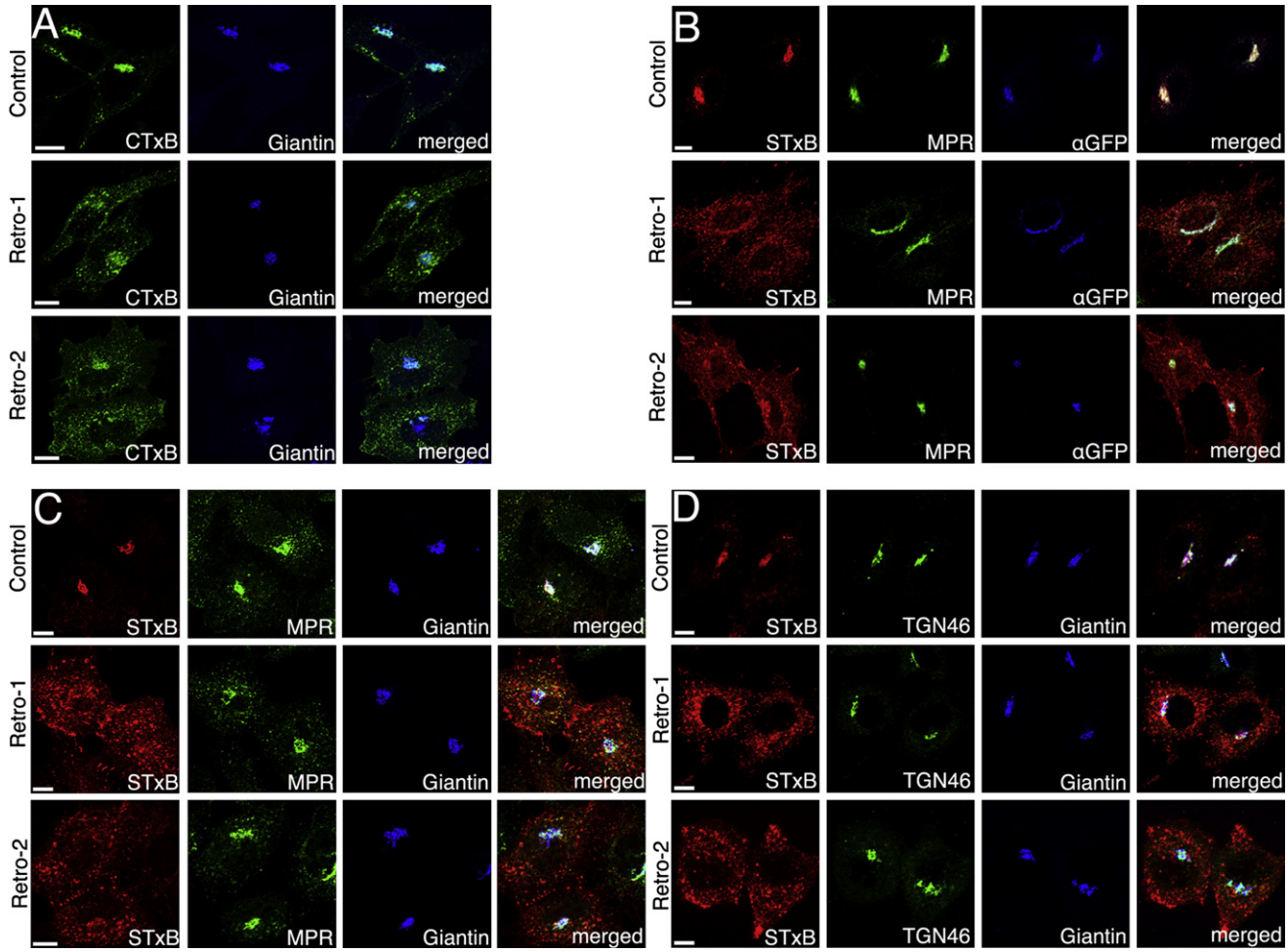

Figure 6. Effects of Retro-1 and Retro-2 on the Retrograde Transport of Various Cargo Proteins

In all conditions, HeLa cells were treated with DMSO (0.04%; control) Retro-1, or Retro-2 (20 μM). For incubation periods, see below.

(A) CTxB trafficking (preincubation of 30 min). After binding, Alexa488-CTxB (4 μg/ml, green) was incubated with HeLa cells for 45 min at 37°C. The cells were fixed and labeled for giantin (blue). Note that CTxB is blocked in peripheral structures in compound-treated cells.

(B) Antibody uptake assay for CI-MPR (preincubation of 60 min): HeLa cells stably expressing GFP-CI-MPR (green) were allowed to internalize surface-bound Cy3-STxB (red) in the presence of anti-GFP antibody (blue) for 40 min at 37°C. Note that the anti-GFP antibody is efficiently transported to the Golgi, in contrast to STxB.

(C) Steady-state localization of CI-MPR: HeLa-cells were incubated with Retro-1 or Retro-2 (20 μM) for 5½ hours at 37°C. After binding of Cy3-STxB (red), cells were incubated for another 45 min at 37°C. The cells were then fixed and labeled for CI-MPR (green) and giantin (blue).

(D) Steady-state localization of TGN46: Cells were treated as in Figure 6C, and labeled for TGN46 (green) and giantin (blue).

Scale bars represent 10 μm.

Retro-1 (middle panel) and Retro-2 (lower panel) only had a minor effect on the steady-state distribution of endogenous CI-MPR (green), while STxB (red) transport was strongly inhibited.

TGN46 is another well-studied retrograde cargo protein of unknown function that like STxB traffics between early endosomes and the TGN (Ghosh et al., 1998; Mallard et al., 1998). As for CI-MPR, we found that the steady-state distribution of TGN46 (green; Figure 6D) was not affected by a 6 hr cell treatment with 20 μM of Retro-1 (middle panel) or Retro-2 (lower panel). Again, it was validated that STxB (red) trafficking was inhibited under these conditions. Clearly, both inhibitors are selective for the retrograde trafficking of exogenous toxins that we have tested here, and do not affect endogenous CI-MPR and TGN46.

Retro-1 and Retro-2 Protect Mice against Intoxication by Ricin

We have found that Retro-1 and Retro-2 selectively inhibit cellular toxin uptake without affecting compartment integrity, endogenous retrograde cargo transport, and a number of other trafficking events. Encouraged by this selectivity, we analyzed whether these compounds could be used to protect mice against lethal ricin challenges. Retro-1 and Retro-2 were nontoxic for animals after intraperitoneal administration of up to

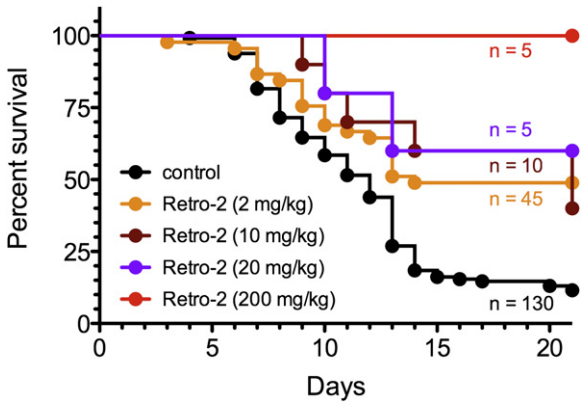

Figure 7. Retro-2 Protects Mice against Ricin Challenge

Comparison of survival curves of mice that were treated with various doses of Retro-2 and then exposed to ricin via the nasal route. In each experiment, treated animals received a single dose of Retro-2 intraperitoneally 1 hr prior to toxin exposure (2 μg/kg by nasal instillation), while control animals received vehicle only prior to ricin administration. The curves for treated animals are statistically different from control as measured by the log rank test ($p < 0.0001$ for 2 mg/kg of Retro-2, orange; $p = 0.015$ for 10 mg/kg, brown; $p = 0.031$ for 20 mg/kg, purple; $p = 0.0007$ for 200 mg/kg, red). See also Figure S7 and Tables S1 and S2.

400 mg/kg (Table S1). A model of ricin intoxication by nasal instillation was developed to mimic exposure by aerosols, a likely modality in bioterror attacks (http://emergency.cdc.gov/agent/ricin/). In this model, a dose of ricin leading to 90% deaths at day 21 (LD_{90}) was used (Figure 7, black curve). The first clinical signs of intoxication appeared within 24 hr. All the mice first got bristly and greasy hairs. From day 2, loss of body weight was observed. At later time points other symptoms were noticed such as prostration, shaking, and respiratory distress, and animals needed to be sacrificed starting from day 7 after exposure. A strong and statistically highly significant protection was observed with a single dose of 2 mg/kg of Retro-2 injected intraperitoneally 1 hr prior toxin challenge (Figure 7, orange curve). Forty-nine percent (n = 45; five independent experiments) of Retro-2-injected mice survived ($p = 0.001$), while in the control group, survival was as low as 11.5% (n = 130, 10 independent experiments). Comparison of survival curves also showed a significant difference (Figure 7; $p < 0.0001$). On the basis of this robust result, complementary experiments were performed with exploratory doses of Retro-2. Survival of mice followed a dose-response relation. Administration of 10 mg/kg (brown curve) and 20 mg/kg (purple curve) of Retro-2 also gave statistically significant levels of protection, compared to the control group ($p = 0.015$, n = 10 and $p = 0.031$, n = 5, respectively), resulting in 60% survival at 20 days (Figure 7). Finally, 200 mg/kg of Retro-2 fully protected mice against ricin challenge ($p = 0.0007$, n = 5) (Figure 7, red curve). Survival curves are shifted toward higher survival numbers according to Retro-2 dose increase. Similarly, the median mortality, at which 50% deaths were observed, is delayed according to dose. These medians were for control, day 12; and for Retro-2 at 2 mg/kg, day 14, and at 10 mg/kg, day 21. At 20 and 200 mg/kg, the value could not be determined because mortality was less than 50%.

The results obtained in vivo with Retro-1 were more difficult to interpret but nevertheless showed some protection with the lowest dose that was used in this study (0.5 mg/kg, blue curve; Figure S7). In this condition, three out of five mice survived, while all of the 14 mice of the control group died ($p = 0.014$). Retro-1 did not have a protective effect at doses of 2, 10, 20, and 200 mg/kg (Figure S7).

In conclusion, we demonstrate that a small molecule can protect animals exposed to a lethal dose of ricin, thereby identifying Retro-2 as a lead compound for the development of inhibitors of toxins that follow the retrograde route.

DISCUSSION

In this study, we used a cell-based HTS assay to identify chemical inhibitors of cell intoxication by ricin. Two compounds with efficacy against both ricin and SLTs were selected. These molecules do not act on the toxins themselves. Rather, they inhibit retrograde transport between early endosomes and the TGN. Such protection of one drug (our small molecule inhibitors) against the action of another (ricin or SLTs) falls under the general phenomena of suppressive drug interactions (Fraser, 1872; Yeh et al., 2009). Obtaining broad-spectrum drugs acting on the host instead of the pathogen may have several advantages: (1) usefulness against new emerging pathogens, (2) new possibilities to act on known pathogens that have become resistant to existing drugs, and (3) reduced risk of acquisition of resistance. The latter point is related to the fact that the pathogen would need to develop a novel mechanism of action to escape the cell-based inhibitor, requiring many adaptive mutations.

The chemical compounds that we have identified, Retro-1 and Retro-2, possess exquisite specificity for the toxins that we have tested. How this specificity is achieved is not yet understood. Nevertheless, one can hypothesize that glycolipids may be involved. Glycolipids indeed are the cellular receptors of SLTs and cholera toxin (Holmgren et al., 1973; Jacewicz et al., 1986) and are required for their internalization and intracellular trafficking (Sandvig et al., 2004). Even if the role of glycolipids in ricin intoxication has been questioned (Spilsberg et al., 2003), other data suggest that they may contribute to the process, in addition to glycoprotein receptors (Lord et al., 2003). When toxins are bound to glycolipids, they interact only with the exoplasmic leaflet of the membrane. In contrast, the endogenous proteins TGN46 (Ponnambalam et al., 1996) and CI-MPR (Glickman et al., 1989) that are not affected by Retro-1 or Retro-2 depend on sorting signals in their cytosolic tails for proper intracellular trafficking. Such disparity between the glycolipid toxin receptors and endogenous protein cargos may explain the difference of susceptibility to Retro-1 and Retro-2. Other explanations such as distinct molecular trafficking requirements must also be considered.

Retro-1 and Retro-2 did not show any additive or synergistic effect, and it is therefore likely that they share a common target. As a first step to target identification, we have screened Retro-1 and Retro-2 for effects on the localization of trafficking machinery at the endosome-TGN interface. Of note, among the 26 factors that have been analyzed, only syntaxin 5 and, to a lesser extent, syntaxin 6 were relocalized from their normal

site of accumulation on perinuclear Golgi membranes. Both of these SNAREs have previously been implicated in the retrograde toxin transport to the TGN (Mallard et al., 2002; Nishimoto-Morita et al., 2009; Tai et al., 2004), and, in agreement with earlier findings (Amessou et al., 2007), we observed here that Shiga toxin was blocked in early endosomes in cells in which syntaxin 5 activity was altered. Whether these SNAREs are direct targets of Retro-1 and Retro-2 and whether their relocalization is directly responsible for the transport inhibition still need to be established. To the least, these findings confirm the exquisite specificity of the inhibitory compounds, provide important leads for target identification, and further establish the early endosome-TGN interface as the site of action of Retro-1 and Retro-2.

Some small molecules have already been identified that inhibit retrograde transport of toxins, such as brefeldin A (Donta et al., 1995), Exo2 (Feng et al., 2004), Golcidide A (Sáenz et al., 2009), and others (Saenz et al., 2007). These compounds rapidly affect compartment morphology, and their effects on trafficking are limited neither to the retrograde route nor to toxins. Animal data have yet to be reported for these compounds.

On cells, Retro-1 and Retro-2 have a much stronger protective effect against SLTs than against ricin. Most likely, ricin can use several mechanisms to traffic between endosomes and the TGN, by binding to a variety of receptors. In contrast, Stx1 and Stx2 only bind to Gb3, and, within a given cell type, may be facing limited molecular redundancy for reaching TGN membranes. Ricin has also been proposed to cross endosomal membranes to reach the cytosol, as an alternative mechanism to retrotranslocation from the ER (Beaumelle et al., 1993). This type of endosomal escape would allow bypassing the retrograde transport requirement.

One of the most striking findings of the current manuscript is the Retro-2-mediated protection of mice from a lethal ricin challenge. Retro-2 therefore appears as a promising candidate for the further development as an antiricin drug. Interfering with ricin after an initial exposure may be of medical interest as ricin progresses through tissues over several days (Cook et al., 2006). In addition, antibodies against ricin can protect mice when administered up to 24 hr after an initial ricin exposure (Pratt et al., 2007).

A surprising result is that Retro-2 is able to protect mice against lethal ricin challenge while its protective factor on cells is only around 3. This may be explained by the steepness of the toxicity curve in mice. Indeed, protection experiments were conducted at 2 μg/kg of ricin per mice, corresponding to one LD_{90} (Figure 7), while in toxicity assay all mice survived at 1 μg/kg (Table S2). Thus, at LD_{90}, a small reduction of toxin efficacy may lead to efficient protection.

At this stage, the reason why in mice Retro-1 does not confer the same protection against ricin as Retro-2 is unclear. Since Retro-1 and Retro-2 were both equally potent at inhibiting retrograde transport and cell intoxication, we suspect that differences in biodistribution and/or pharmacokinetics are responsible for the limited in vivo activity of Retro-1. One must consider that Retro-1 and Retro-2 are nonoptimized hits and that chemical engineering may further improve their in vivo activity.

In the case of SLTs, disease leading to life-threatening hemolytic-uremic syndrome develops over days (Tarr et al., 2005), and to date no proven safe treatment exists for infection by SLT-producing *E. coli* strains and the prevention of SLT-mediated complications, other than supportive care. Moreover, the use of antibiotics seems to exacerbate the disease, possibly by inducing bacterial lysis and increased release of toxins. Therefore, the development of Retro-2 may also be of interest in this pathology. More generally, our study identifies the retrograde route as a potential therapeutic target for the prevention of pathological manifestations that are caused by a variety of toxins that rely on retrograde trafficking to reach their intracellular targets. Among the most prominent of these toxins are ricin, SLTs, and cholera toxin from *Vibrio cholerae* as shown here, but also exotoxin A from *Pseudomonas aeruginosa* and subtilase cytotoxin and heat-labile enterotoxin from *E. coli*.

EXPERIMENTAL PROCEDURES

A list of chemicals and materials can be found in the Extended Experimental Procedures.

High-Throughput Screening

The HTS assay protocol is described in detail in the Extended Experimental Procedures. In brief, A549 cells were grown in Cytostar T scintillating microplates (GE) with incorporated scintillator. Ricin was added to each well of library compounds microplates. The commercial Chembridge DIVERset library, consisting of 16,480 compounds that were tested at a final concentration of 25 μM, was screened. The mix was then transferred onto the cells (final ricin concentration: 10^{-10} M). After 20 hr, cells were grown for an additional 7 hr in the presence of ^{14}C-leucine. Data were normalized as percentage inhibitor relative to positive control. Active compounds were defined as those exhibiting an inhibiting activity of greater than 10%. The most efficient concentrations of active compounds were defined as those that exhibit the best cellular protection index (EC_{50}drug/EC_{50}toxin ratio) without exhibiting cytotoxicity.

HeLa Cells and Intoxication Assay

HeLa cells were maintained at 37°C under 5% CO_2 in Dulbecco's modified Eagle's medium (DMEM; Invitrogen) supplemented with 10% fetal bovine serum, 4.5 g/l glucose, 0.01% penicillin-streptomycin, 4 mM glutamine, and 5 mM pyruvate. HeLa cells were seeded at 20,000 cells per well in 96-well plates and grown overnight. After incubation with 20 μM of compound (or 0.04% DMSO) for 30 min at 37°C, cells were challenged with increasing doses of ricin (4 hr), Stx1, or Stx2 (1 or 4 hr), in the continued presence of compounds. Protein biosynthesis was determined 1 hr later by measuring the incorporation of radiolabeled methionine into acid-precipitable material, as previously described (Amessou et al., 2007).

The mean percentage of protein biosynthesis was determined and normalized from duplicate wells. All values are expressed as means ± SEM. Data were fitted with Prism v5 software (Graphpad, San Diego, CA) to obtain the 50% effective toxin concentration (EC_{50}). EC_{50} values and protection factor (i.e., EC_{50} ratio = EC_{50}drug/EC_{50}toxin) were determined by the nonlinear regression dose-response EC_{50} shift equation. The goodness of fit for each toxin and drug was assessed by R^2 and confidence intervals.

Immunofluorescence and Electron Microscopy

For immunofluorescence experiments, compound-treated cells were first incubated with Cy3-STxB (0.5 μg/ml) or Alexa488-CTxB (4 μg/ml) for 30 min on ice, followed by 45 min at 37°C in the continued presence of compounds (20 μM). Cells were fixed, immunolabeled with antibodies corresponding to the indicated proteins, and imaged with a Leica TCS SP2 confocal microscope with HCX PL APO objectives (100×/1.40–0.7 and 63×/1.32–0.60, Leica Microsystems, Mannheim, Germany). Maximum projections of six to eight optical Z slices (300 nm Z separation) are shown. Overlap was quantified for each condition on 6 cells on a total of 200–300 structures by determining the fraction of compartment marker-positive structures that were also labeled for STxB.

For electron microscopy, control cells or cells treated for 30 min at 37°C with 20 μM of Retro-1 or Retro-2 were put on ice, incubated for 30 min with 0.5 μM

of STxB, and then shifted for 45 min to 37°C. The latter two steps were done in the continued presence of the compounds. The cells were fixed with a mixture of 2% PFA and 0.2% glutaraldehyde in 0.1 M phosphate buffer (pH 7.4) and processed for ultracryomicrotomy and double-immunogold labeled with protein A conjugated to 10 nm gold (PAG10) or 15 nm gold (PAG15). Sections were observed under an electron microscope (Philips CM120; FEI Company), and digital acquisitions were made with a numeric camera (Keen View; Soft Imaging System).

Sulfation Assay

The sulfation assay was performed as previously described (Amessou et al., 2006). In brief, a STxB variant termed STxB-$Sulf_2$ that bears a tandem of protein sulfation recognition sites was bound to cells on ice. After washing, the cells were incubated for 20 min at 37°C in the presence of ^{35}S-sulfate (480 μCi/ml), STxB was immunoprecipitated, and sulfation was quantified by autoradiography.

Endocytosis and Recycling Assays

STxB and Tf were biotinylated with NHS-SS-biotin as previously described (Amessou et al., 2006). Compound-treated (20 μM, 30 min at 37°C) HeLa cells were detached with 2 mM EDTA/PBS, followed by the incubation with STxB-SS-biotin (5 μg/ml) and Tf-SS-biotin (20 μg/ml) on ice. After washing, cells were incubated at 37°C for the indicated times. Biotin on surface-exposed STxB-SS-biotin and Tf-SS-biotin was cleaved on ice by treatment with the non-membrane-permeable reducing agent MESNA (2-mercaptoethansulfonic acid, 100 mM). Under these conditions, internalized STxB-SS-biotin and Tf-SS-biotin are protected against reductive cleavage. After inactivation of MESNA with iodoacetamide (150 mM) and cell lysis, biotinylated STxB and Tf were quantified by ELISA with anti-STxB mAb 13C4, anti-Tf mAb H68.4, and streptavidin-HRP.

Recycling of Tf was determined as follows: HeLa cells were incubated with Tf-SS-biotin (40 μg/ml) for 60 min at 37°C. The cells were washed, and incubation was continued at 37°C for the indicated times in the absence of Tf-SS-biotin. The remaining cell-associated biotinylated Tf was quantified at each time point by ELISA, as described above.

EGF Degradation

^{125}I-EGF was bound on ice to compound-treated (20 μM, 30 min at 37°C) HeLa cells. After incubation in the continued presence of the compounds for the indicated times at 37°C in serum-free HEPES culture medium, TCA-precipitable counts were determined in culture medium and cell lysates, essentially as described (Mallard et al., 1998). One hundred percent indicates the quantitative transformation of ^{125}I-EGF into TCA soluble counts.

Anterograde VSVG Transport

The anterograde transport of GFP-VSVG^{ts045} was measured on control and compound-treated cells, as described (Amessou et al., 2007). In brief, cells were transfected with an expression plasmid containing *GFP-VSVG^{ts045}* cDNA, using a calcium phosphate transfection kit (Invitrogen) and incubated overnight at nonpermissive temperature (40°C). Under these conditions, the misfolded protein accumulates in the ER. Subsequently, detached cells were treated with carrier (0.04% DMSO), Retro-1 (20 μM), Retro-2 (20 μM), or brefeldin A (18 μM) for 30 min at 37°C. VSVG folding and subsequent transport of the folded protein to the Golgi apparatus and plasma membrane was initiated by shifting cells to 32°C in the presence of compounds. Expression at the plasma membrane was quantified 2 hr later by flow cytometry on a FacsCalibur multipurpose flow cytometer with an antibody directed against the extracellular domain of VSVG.

In Vivo Experiments

Animal studies were done at French Health Products Safety Agency (Afssaps) animal care facility and in compliance with Afssaps committee policies according to European regulations. Pathogen-free 6-week-old female Balb/c mice were purchased from Charles River Laboratories (L'Arbresle, France). Experiments were performed according to good laboratory practice, ISO 17025 standard, and the guide for the care and use of laboratory animals. Environmental parameters are in accordance with European directive 86/609/CEE. Mice were housed under a 12 hr light-dark cycle and fed a standard diet ad libidum. Standardized groups of mice were injected intraperitoneally with 500 μl of sterile saline solution (0.9% NaCl) supplemented with 1%–10% DMSO alone (control) or with various doses of Retro-1 or Retro-2 one hour prior to toxin administration.

Mice were anesthetized by intraperitoneal injection (100 μL) of ketamine (1.15 mg final) -rompun (xylazine, 0.28 mg final) solution and exposed to 50 μl of ricin (2 μg/kg) by intranasal instillation corresponding to one LD_{90} at day 21. Each drug-treated group contained five to ten mice, and normal controls contained ten mice. Survival was recorded daily.

Data for mice in each test group were compared to those for untreated ricin-challenged mice by the log rank test (Prism, Graphpad, San Diego, CA), and p values ≤ 0.05 were considered statistically significant.

SUPPLEMENTAL INFORMATION

Supplemental Information includes Extended Experimental Procedures, seven figures, and three tables and can be found with this article online at doi:10.1016/j.cell.2010.01.043.

ACKNOWLEDGMENTS

This work was supported by grants from the European Union (Cancerimmunotherapy), Project ToxScreen, and the Commissariat a l'Energie Atomique et aux Energies Alternatives. B.S. was supported by Association pour la Recherche sur le Cancer. We are grateful to François Becher, Elodie Duriez and Eric Ezan for measurement of the enzymatic activity of ricin, Annie El Zaouk, Philippe Chabert, and Emmanuel Intsaby for technical help with mouse experiments, Anne Bonhoure for help with ricin purification, Séverine Hebbe for chemical synthesis of Retro-2, and Jennifer Martinez and Michel Petitjean for technical help. The following colleagues kindly provided us with reagents (further details are in the Extended Experimental Procedures): Georges Bismuth, Juan Bonifacino, Michel Bornens, Frances Brodsky, Paul Gleeson, Jennifer Hirst, Bernard Hoflack, Wanjin Hong, Michael Marks, Kazuhisa Nakayama, Andrew Peden, Franck Perez, Suzanne Pfeffer, Lynne Roberts, and Harald Stenmark.

Received: July 30, 2009
Revised: December 14, 2009
Accepted: January 25, 2010
Published: April 15, 2010

REFERENCES

Amessou, M., Popoff, V., Yelamos, B., Saint-Pol, A., and Johannes, L. (2006). Measuring retrograde transport to the trans-Golgi network. Curr. Protoc. Cell Biol. *Chapter 15*, Unit 15.10.

Amessou, M., Fradagrada, A., Falguières, T., Lord, J.M., Smith, D.C., Roberts, L.M., Lamaze, C., and Johannes, L. (2007). Syntaxin 16 and syntaxin 5 are required for efficient retrograde transport of several exogenous and endogenous cargo proteins. J. Cell Sci. *120*, 1457–1468.

Arighi, C.N., Hartnell, L.M., Aguilar, R.C., Haft, C.R., and Bonifacino, J.S. (2004). Role of the mammalian retromer in sorting of the cation-independent mannose 6-phosphate receptor. J. Cell Biol. *165*, 123–133.

Astoul, E., Edmunds, C., Cantrell, D.A., and Ward, S.G. (2001). PI 3-K and T-cell activation: limitations of T-leukemic cell lines as signaling models. Trends Immunol. *22*, 490–496.

Audi, J., Belson, M., Patel, M., Schier, J., and Osterloh, J. (2005). Ricin poisoning: a comprehensive review. JAMA *294*, 2342–2351.

Beaumelle, B., Alami, M., and Hopkins, C.R. (1993). ATP-dependent translocation of ricin across the membrane of purified endosomes. J. Biol. Chem. *268*, 23661–23669.

Bonifacino, J.S., and Hurley, J.H. (2008). Retromer. Curr. Opin. Cell Biol. *20*, 427–436.

Bonifacino, J.S., and Rojas, R. (2006). Retrograde transport from endosomes to the trans-Golgi network. Nat. Rev. Mol. Cell Biol. *7*, 568–579.

Cook, D.L., David, J., and Griffiths, G.D. (2006). Retrospective identification of ricin in animal tissues following administration by pulmonary and oral routes. Toxicology *223*, 61–70.

Donta, S.T., Tomicic, T.K., and Donohue-Rolfe, A. (1995). Inhibition of Shiga-like toxins by brefeldin A. J. Infect. Dis. *171*, 721–724.

Feng, Y., Jadhav, A.P., Rodighiero, C., Fujinaga, Y., Kirchhausen, T., and Lencer, W.I. (2004). Retrograde transport of cholera toxin from the plasma membrane to the endoplasmic reticulum requires the trans-Golgi network but not the Golgi apparatus in Exo2-treated cells. EMBO Rep. *5*, 596–601.

Fraser, T.R. (1872). Lecture on the antagonism between the actions of active substances. Br. Med. J. *2*, 485–487.

Ghosh, R.N., Mallet, W.G., Soe, T.T., McGraw, T.E., and Maxfield, F.R. (1998). An endocytosed TGN38 chimeric protein is delivered to the TGN after trafficking through the endocytic recycling compartment in CHO cells. J. Cell Biol. *142*, 923–936.

Ghosh, P., Dahms, N.M., and Kornfeld, S. (2003). Mannose 6-phosphate receptors: new twists in the tale. Nat. Rev. Mol. Cell Biol. *4*, 202–212.

Glickman, J.N., Conibear, E., and Pearse, B.M. (1989). Specificity of binding of clathrin adaptors to signals on the mannose-6-phosphate/insulin-like growth factor II receptor. EMBO J. *8*, 1041–1047.

Hay, J.C., Klumperman, J., Oorschot, V., Steegmaier, M., Kuo, C.S., and Scheller, R.H. (1998). Localization, dynamics, and protein interactions reveal distinct roles for ER and Golgi SNAREs. J. Cell Biol. *141*, 1489–1502.

Holmgren, J., Lönnroth, I., and Svennerholm, L. (1973). Tissue receptor for cholera exotoxin: postulated structure from studies with GM1 ganglioside and related glycolipids. Infect. Immun. *8*, 208–214.

Hunyady, L., Baukal, A.J., Gaborik, Z., Olivares-Reyes, J.A., Bor, M., Szaszak, M., Lodge, R., Catt, K.J., and Balla, T. (2002). Differential PI 3-kinase dependence of early and late phases of recycling of the internalized AT1 angiotensin receptor. J. Cell Biol. *157*, 1211–1222.

Jacewicz, M., Clausen, H., Nudelman, E., Donohue-Rolfe, A., and Keusch, G.T. (1986). Pathogenesis of shigella diarrhea. XI. Isolation of a shigella toxin-binding glycolipid from rabbit jejunum and HeLa cells and its identification as globotriaosylceramide. J. Exp. Med. *163*, 1391–1404.

Johannes, L., and Popoff, V. (2008). Tracing the retrograde route in protein trafficking. Cell *135*, 1175–1187.

Johannes, L., and Römer, W. (2010). Shiga toxins—from cell biology to biomedical applications. Nat. Rev. Microbiol. *8*, 105–116.

Liger, D., vanderSpek, J.C., Gaillard, C., Cansier, C., Murphy, J.R., Leboulch, P., and Gillet, D. (1997). Characterization and receptor specific toxicity of two diphtheria toxin-related interleukin-3 fusion proteins DAB389-mIL-3 and DAB389-(Gly4Ser)2-mIL-3. FEBS Lett. *406*, 157–161.

Lord, M.J., Jolliffe, N.A., Marsden, C.J., Pateman, C.S., Smith, D.C., Spooner, R.A., Watson, P.D., and Roberts, L.M. (2003). Ricin. Mechanisms of cytotoxicity. Toxicol. Rev. *22*, 53–64.

Mallard, F., Antony, C., Tenza, D., Salamero, J., Goud, B., and Johannes, L. (1998). Direct pathway from early/recycling endosomes to the Golgi apparatus revealed through the study of shiga toxin B-fragment transport. J. Cell Biol. *143*, 973–990.

Mallard, F., Tang, B.L., Galli, T., Tenza, D., Saint-Pol, A., Yue, X., Antony, C., Hong, W.J., Goud, B., and Johannes, L. (2002). Early/recycling endosomes-to-TGN transport involves two SNARE complexes and a Rab6 isoform. J. Cell Biol. *156*, 653–664.

Nishimoto-Morita, K., Shin, H.W., Mitsuhashi, H., Kitamura, M., Zhang, Q., Johannes, L., and Nakayama, K. (2009). Differential effects of depletion of ARL1 and ARFRP1 on membrane trafficking between the trans-Golgi network and endosomes. J. Biol. Chem. *284*, 10583–10592.

Ponnambalam, S., Girotti, M., Yaspo, M.L., Owen, C.E., Perry, A.C., Suganuma, T., Nilsson, T., Fried, M., Banting, G., and Warren, G. (1996). Primate homologues of rat TGN38: primary structure, expression and functional implications. J. Cell Sci. *109*, 675–685.

Pratt, T.S., Pincus, S.H., Hale, M.L., Moreira, A.L., Roy, C.J., and Tchou-Wong, K.M. (2007). Oropharyngeal aspiration of ricin as a lung challenge model for evaluation of the therapeutic index of antibodies against ricin A-chain for post-exposure treatment. Exp. Lung Res. *33*, 459–481.

Saenz, J.B., Doggett, T.A., and Haslam, D.B. (2007). Identification and characterization of small molecules that inhibit intracellular toxin transport. Infect. Immun. *75*, 4552–4561.

Sáenz, J.B., Sun, W.J., Chang, J.W., Li, J., Bursulaya, B., Gray, N.S., and Haslam, D.B. (2009). Golgicide A reveals essential roles for GBF1 in Golgi assembly and function. Nat. Chem. Biol. *5*, 157–165.

Sandvig, K., and van Deurs, B. (2005). Delivery into cells: lessons learned from plant and bacterial toxins. Gene Ther. *12*, 865–872.

Sandvig, K., Spilsberg, B., Lauvrak, S.U., Torgersen, M.L., Iversen, T.G., and van Deurs, B. (2004). Pathways followed by protein toxins into cells. Int. J. Med. Microbiol. *293*, 483–490.

Snider, M.D., and Rogers, O.C. (1985). Intracellular movement of cell surface receptors after endocytosis: resialylation of asialo-transferrin receptor in human erythroleukemia cells. J. Cell Biol. *100*, 826–834.

Spilsberg, B., Van Meer, G., and Sandvig, K. (2003). Role of lipids in the retrograde pathway of ricin intoxication. Traffic *4*, 544–552.

Tai, G., Lu, L., Wang, T.L., Tang, B.L., Goud, B., Johannes, L., and Hong, W. (2004). Participation of the syntaxin 5/Ykt6/GS28/GS15 SNARE complex in transport from the early/recycling endosome to the trans-Golgi network. Mol. Biol. Cell *15*, 4011–4022.

Tarr, P.I., Gordon, C.A., and Chandler, W.L. (2005). Shiga-toxin-producing Escherichia coli and haemolytic uraemic syndrome. Lancet *365*, 1073–1086.

Waguri, S., Dewitte, F., Le Borgne, R., Rouillé, Y., Uchiyama, Y., Dubremetz, J.F., and Hoflack, B. (2003). Visualization of TGN to endosome trafficking through fluorescently labeled MPR and AP-1 in living cells. Mol. Biol. Cell *14*, 142–155.

Yeh, P.J., Hegreness, M.J., Aiden, A.P., and Kishony, R. (2009). Drug interactions and the evolution of antibiotic resistance. Nat. Rev. Microbiol. *7*, 460–466.

Zhang, T., and Hong, W. (2001). Ykt6 forms a SNARE complex with syntaxin 5, GS28, and Bet1 and participates in a late stage in endoplasmic reticulum-Golgi transport. J. Biol. Chem. *276*, 27480–27487.